Front. Optoelectron. 2017, 10(2): 117–123
DOI 10.1007/s12200-017-0712-x

RESEARCH ARTICLE

Fabricate organic thermoelectric modules use modified PCBM and PEDOT:PSS materials

Feng GAO, Yuchun LIU, Yan XIONG, Ping WU, Bin HU, Ling XU (✉)

Wuhan National Laboratory for Optoelectronics, Huazhong University of Science and Technology, Wuhan 430074, China

Abstract In this paper, we fabricated an organic thermoelectric (TE) device with modified [6,6]-phenyl-C61-butyric acid methyl ester (PCBM) and poly(3,4-ethylenedioxythiophene) polystyrene sulfonate (PEDOT:PSS); the device showed good stability in air condition. For n-leg, PCBM were doped with acridine orange base (3,6-bis (dimethylamino)acridine) (AOB) and 1,3-dimethyl-2,3-dihydro-1H-benzoimidazole (N-DMBI). Co-doped PCBM utilizes synergistic effects of AOB and N-DMBI, resulting in excellent electrical conductivity and Seebeck coefficient values reaching 2 S/cm and −500 μV/K, respectively, at room temperature with dopant molar ratio of 0.11. P-type leg used modified PEDOT:PSS. Based on modified PCBM and PEDOT:PSS materials, we fabricated a TE module device with 48 p-type and n-type thermocouple and tested their output voltage, short current, and power. Output voltage measured ~0.82 V, and generated power reached almost 945 μW with 75 K temperature gradient at 453 K hot-side temperature. These promising results showed potential of modified PEDOT and PCBM as TE materials for application in device optimization.

Keywords organic thermoelectric generator, thermocouple, poly(3,4-ethylenedioxythiophene) polystyrene sulfonate (PEDOT-PSS), [6.6]-phenyl-C61butyric acid methyl ester (PCBM)

1 Introduction

Since Thomas John Baker, a German scientist, discovered Seebeck effect in 1821, scientists constantly searched for thermoelectric (TE) materials for energy application. Some researchers discovered inorganic TE materials, such as Bi_2Te_3 and SnSe, with good TE properties and extensive application in energy field [1–4]. In comparison with inorganic TE materials, development of organic TE materials is retarded by poor stability of their properties, such as high temperature, that limit their application; processing of organic materials is also difficult compared with inorganic ones. However, organic TE materials and devices feature their own advantages, e.g., abundant resources, low-cost synthesis, mechanical flexibility, and solution processability over large areas [5–7]. Currently, increasing number of scientists explore TE properties of organic materials [8–13]. On the one hand, electrical conductivity of organic materials can be controlled by methods such as doping, on the other hand, thermal conductivity can be controlled by designing molecular structures [14–17]. To increase electrical conductivity, many methods were reproved, for example, using composite materials to fill materials with high electrical conductivity [18–20] and preparing new composite structural materials [21–24]. These methods only bear significance in controlling P-type TE materials, including poly(3,4-ethylenedioxythiophene) (PEDOT), which show good stability in air [25,26]; however, difficulty arises from using these methods to modify TE properties of n-type materials. Recently, some new methods were reported for modification of n-type TE materials, for example, using doping and phase separation method to process large-sized materials [27] and modifying side chains of molecules; both methods can provide n-type TE materials with good stability in air [28]. Phenyl-C61-butyric acid methyl ester (PCBM) is one of the promising n-type TE materials, it presents excellent phase segregation characteristic and broad application prospects in field of organic solar cells [29–33]. Pure PCBM features high thermal conductivity [34,35]; thus, this material cannot be easily processed by the solution method. When used as filler material, PCBM blends with other composites materials and easily results in low thermal conductivity (κ), realizing high electrical conductivity (σ) and high Seebeck coefficient (S). In some literature [36–38] that reported some methods in modifying PCBM, acridine orange base (3,6-bis(dimethylamino)

Received March 22, 2017; accepted May 4, 2017

E-mail: xuling@mail.hust.edu.cn

acridine) (AOB) and 1,3-dimethyl-2-phenyl-2,3-dihydro-1H-benzoimidazole (N-DMBI)-doped PCBM resulted in high electrical conductivity, reaching ~4 and ~5.3 S/cm, respectively. However, these materials cannot simultaneously obtain high Seebeck coefficient. Seebeck coefficient of N-DMBI-doped PCBM is smaller than that of AOB-doped PCBM. In this article, we selected AOB and N-DMBI-co-doped PCBM, because it can simultaneously show high electrical conductivity and Seebeck coefficient and good stability by doping in air condition [39]. For p-type TE materials, we selected modified PEDOT:polystyrene sulfonate (PSS) as p-type leg. Finally, we fabricated p-type and n-type TE modules and tested their output voltage and output power.

2 Experiments

In our experiment, we first dealt with PCBM and PEDOT:PSS. We used AOB and N-DMBI-co-doped PCBM and purificatory PEDOT:PSS materials. To process PCBM, we combined AOB and N-DMBI with PCBM to perform simultaneous co-evaporation. Singly doped PCBM and PCBM co-doped with AOB and N-DMBI presented dopant molar ratios (MRs) ranging from 0.007 to 0.7. Doping ration of AOB, N-DMBI, and PCBM were calculated by their molar masses, which measure 265.4, 240.3, and 720.6 g/mol, respectively. During preparation of PCBM, base pressure of vacuum chamber was 5×10^{-5} Pa, evaporator sources comprised two copper electrodes, and their spacing spanned 5 mm. Organic materials were evaporated on glass substrate, thermal evaporation rate reached 0.015 nm/s, and thickness of thin film measured 200–300 nm. Temperature of glass substrate was 298 K. Metal electrode of Au was evaporated on organic materials, with length measuring 20 mm and thickness reaching 60 nm. Maximal evaporation rate and doping concentration were monitored by two quartz crystal monitors.

PEDOT:PSS (including dispersion) were purchased from the Sigma-Aldrich Company. We spin-coated PEDOT:PSS on glass substrate at a speed 1000 rpm. Thin film thickness totaled 1 μm. PEDOT:PSS consisted of 10 g PEDOT:PSS dispersion, 0.3 g sorbitol, 0.5 g N-methyl-pyrrolidone (NMP), and 10 g isopropanol. Then, 1 mm glass fiber filter was used to filter materials to obtain a smoother thin film. Finally, we heated the thin film for 5 min at 474 K to remove sorbitol and NMP; this process can increase electrical conductivity of PEDOT:PSS thin film.

Electrical conductivity and Seebeck coefficient were measured using Keithley 2400 (Agilent Technologies). Thermal absorption is a deferring process. To remove system errors, when thermal absorption reaches saturation, measured Seebeck voltages are usually averaged after 10 min. In our measurement, temperature difference reached 8 K between hot side and cold side. Second, we kept the temperature constant, swapped hot-side and cold-side temperatures, and measured Seebeck coefficient again to further exclude systematic errors by averaging twice-measured Seebeck coefficient ($S = \Delta V/\Delta T$). Seebeck coefficient thus refers to twice-averaged values. During Seebeck measurements, indium tin oxide (ITO) substrate was heated, and unheated side was cooled using a fan to maintain constant temperature. Substrate temperatures were within the range of t = 300–475 K. Table 1 shows some parameters of modified PEDOT:PSS and PCBM.

Measurements in TE experiment may result in some errors, which are generated by two primary causes: one is the different potential generated by metal wires when measuring temperature, and the other is system error generated by uneven heating. Therefore, standard deviations of performance parameters must be calculated. For errors of metal electrode, temperature increased at the interface between sensor and sample at less than 2°C. This temperature increase induced changes in voltage drop of sensor element. We eliminated this error in data transactions. In case of Al or Au metal wires, we used Al and Au material with the same length to measure their different potentials for correcting corresponding temperatures. Errors caused by uneven heating are usually inevitable in experiments. Thus, we computed standards deviations to eliminate their effects. Standard deviations for Seebeck coefficient measurement, electrical conductivity, output voltage, and short current reached 3.3%, 2%, 2.4%, and 3.1%, respectively.

3 Results and discussion

Figure 1(a) shows conductivity of singly-doped and PCBM co-doped with AOB and N-DMBI under various doping concentration at t = 298 K in a double-logarithmic scale. Electrical conductivity of undoped PCBM is $\sigma = 10^{-8}$ S/cm [37], whereas that of doped PCBM is several orders of magnitude higher. Electrical conductivities of both single-doped and double-doped PCBM increased with increasing dopant concentration. Compared with AOB and N-DMBI doping, electrical conductivity of N-DMBI-doped PCBM increased by 4–5 orders of magnitude than that of pure PCBM. Electrical conductivity of

Table 1 Electrical conductivity, Seebeck coefficient, and power factor (PF) of modified PEDOT:PSS and PCBM at room temperature

sample	σ/(S·cm^{-1})	S/(μV·K^{-1})	PF/(μW·m^{-1}·K^{-2})
PEDOT:PSS	10±0.1	300±5	9±0.25
AOB and N-DMBI-co-doped PCBM	2±0.1	−500±5	1±0.25

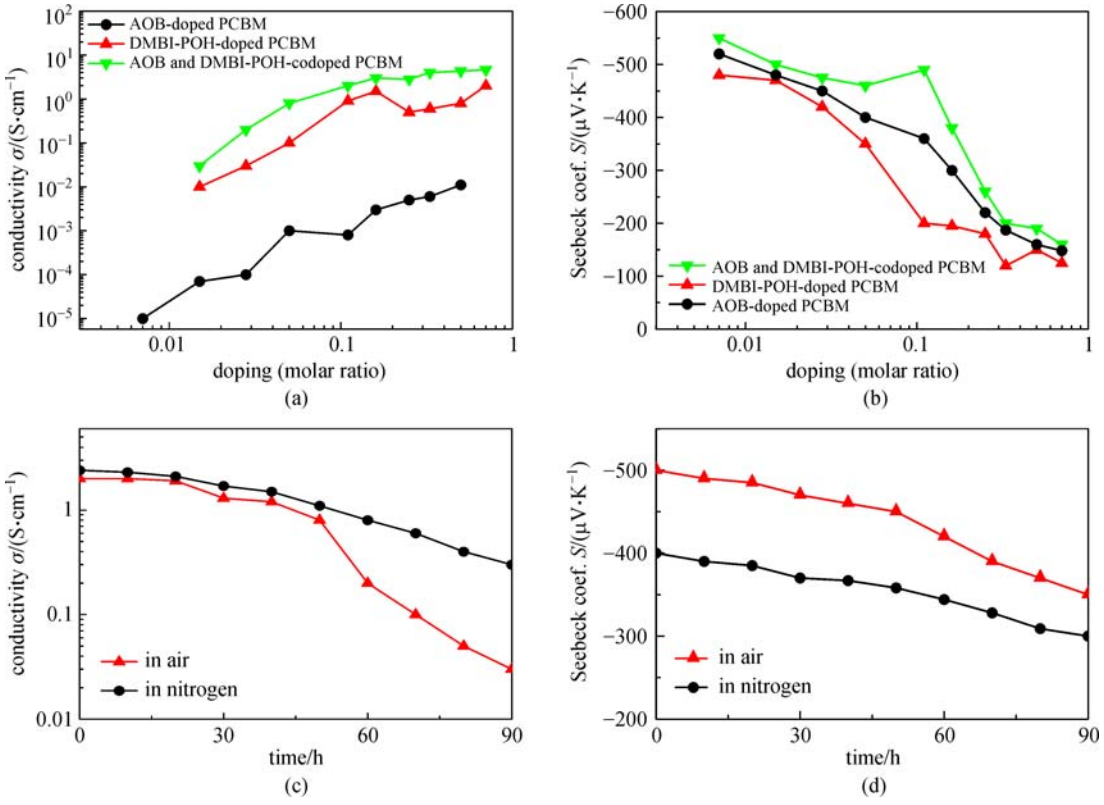

Fig. 1 Seebeck coefficient (a) and electrical conductivity (b) after doping with AOB, N-DMBI, and combined AOB and N-DMBI. Samples doped with AOB and N-DMBI were fabricated by thermal evaporation at varying doping molar ratios (MR) (from 0.07 to 0.7). (c) and (d) Performance stability tests of AOB and N-DMBI-doped PCBM samples. Samples were exposed to room air or nitrogen environment condition. Doping MR is 0.11

AOB-doped PCBM increased by 2–3 orders magnitude than that of pure PCBM. Maximal value of N-DMBI-doped PCBM got σ= 5 S/cm (measured at MR = 0.7).

Changes in electrical conductivity of AOB-doped PCBM ranged from 10^{-5} to 10^{-2} S/cm, and Seebeck coefficient varied from −520 to −148 μV/K when molar concentration of dopant changed from 0.007 to 0.7 at room temperature. Side chain of AOB material features a nitrogen ion, which serves as a primary electron donor. When PCBM was doped with AOB, PCBM accepted an electron from nitrogen ions, elevating Fermi energy close to energy level of lowest energy unoccupied molecular orbital of PCBM and increasing electrical conductivity. As electron donor, nitrogen ion also recombined holes (original ion); this effect decreased the number of free carriers, resulting in increased Seebeck coefficient than that of undoped PCBM.

Electrical conductivity of N-DMBI-doped PCBM (5 S/cm) is higher than that of AOB-doped PCBM. However, Seebeck coefficient of N-DMBI-doped PCBM is slightly lower than that of AOB-doped material. This observation resulted from addition of dense charge carriers that increased electrical conductivity, especially that of N-DMBI-doped PCBM. Charge carriers were distributed along a manifold of states in energy and space, thus leading to their transport along denser parts of the system. After doping of PCBM by N-DMBI, low-lying localized states were filled, significantly increasing density and mobility of charge carriers. Therefore, electrical conductivity increased. Some literature reported this view [40–42], e.g., in organic field-effect transistor devices, which are filled by gate bias.

Seebeck coefficient is negative for PCBM system co-doped with AOB and N-DMBI. Hence, in doping PCBM systems, electrons served as primary charge carriers. Seebeck coefficient decreased with increasing dopant concentration and also exhibited correlation with energy difference between transport level and Fermi-level. Energy difference in AOB-doped PCBM was smaller than that of N-DMBI-doped PCBM, indicating that concentration of charge carrier is also smaller in AOB-doped than in N-DMBI-doped PCBM. Therefore, Seebeck coefficient of AOB-doped PCBM is higher than that of N-DMBI. Overall, PF of N-DMBI-doped PCBM was better than that of AOB-doped PCBM, because electrical conductivity of N-DMBI doping was higher than that of AOB-doping.

When AOB and N-DMBI were co-doped in PCBM, combination of AOB and N-DMBI improved electrical

conductivity and Seebeck effect behavior compared with single doping with AOB or N-DMBI. Maximum electrical conductivity measured 5 S/cm (MR = 0.7), and maximum Seebeck coefficient totaled −550 μV/K (MR = 0.007). In codoping system, nitrogen ions served as primary electron donors on AOB sidewalls. Simultaneously, nitrogen ions also provided hole acceptors on N-DMBI. After co-doping of PCBM, electron and hole recombination action led to decreased concentration of charge carrier and increased Seebeck coefficient. On the other hand, low-lying localized states were filled, leading to energy difference between transport levels, and Fermi-level was decreased by synergistic effects of codoping, leading to increased mobility and electrical conductivity of co-doping than single doping with AOB or N-DMBI.

To determine stability of device by doping with AOB and N-DMBI, related samples were placed in air or nitrogen environments. Meanwhile, all samples were placed in nitrogen environment over 2 days (~ 48 h). Afterward, electrical conductivity and Seebeck coefficient both decreased rapidly, as shown in Figs. 1(c) and 1(d). Samples were relatively stable when placed in a glove box. Oxygen may cause rapid deterioration of TE characteristics. We expected degeneration by oxygen or as effect of water. Seebeck coefficient value reached 10 μV/K at room temperature for pure PCBM, but when placed in air, Seebeck coefficient dramatically changed to ~400 μV/K. After doping by AOB and N-DMBI, Seebeck coefficient and electrical conductivity both increased. Seebeck coefficient was higher in air than in nitrogen conditions, whereas changes in electrical conductivity was minimal in nitrogen condition for AOB and N-DMBI-codoped samples. We also tested effects of water on PCBM. We fabricated PCBM solutions with higher concentrations of up to 5 mg PCBM per mL of water and observed that Seebeck coefficient increased to −200 μV/K, whereas electrical conductivity decreased rapidly. Therefore, water poses more significant effect than oxygen.

For single thermocouple model, as shown in Fig. 2(a), p- and n-type devices were connected by ITO. PEDOT:PSS was heat-treated, followed by spin-coating onto an ITO glass substrate. Then, we erased one half PEDOT:PSS by using ethyl alcohol on ITO and covering the cleaned part with AOB- and N-DMBI-codoped PCBM by thermal evaporation. Lastly, Au and Al electrodes were deposited on top of PEDOT:PSS and PCBM devices, respectively, forming the final ITO/PEDOT:PSS/Au and ITO/ PCBM/ Al TE devices on the same ITO glass substrate. Effective length of single p-type or n-type devices measured 5 mm, and width spanned 2 mm. Active area of p- or n-type single devices reached 10 mm^2. As shown in Fig. 2 (b), we built a TE module with 48 legs based on PEDOT:PSS and doped PCBM materials. First, 3 mm × 3 mm AlN wafer was used as substrate. A total of 48 bottom silver electrodes were inkjet-printed onto ultraviolet/ozone-treated substrates, each 0.35 mm × 0.25 mm and 0.1 mm apart. Then, compressed p- and n-type polymer samples (0.3 mm × 0.2 mm × 1 mm) were placed in a small check with 60 nm evaporated Au layer on one side and were adhered to bottom substrate using silver paste. PEDOT:PSS functioned as the p-leg, and n-leg consisted of AOB and N-DMBI-codoped PCBM. As depicted in Figs. 3(a) and 3(b), voltage and current of fabricated TE devices and modules were measured at different temperatures. At Δt = 75 K, output voltage and current of TE modules measured 0.82 V and 11.52 mA, respectively.

Figure 4(a) shows maximum power output of TE module with different load resistances. Useful power outputs of PEDOT:PSS and PCBM thermocouple with various load resistances were measured at hot-side temperatures of 373 and 453 K, respectively. Temperature differences reached 50 and 75 K, respectively. This all-organic TE module provides a maximum power output of 945 μW when hot-side temperature is 453 K, and temperature difference is 75 K. Figure 4(b) shows maximum output power per area of a PCBM and

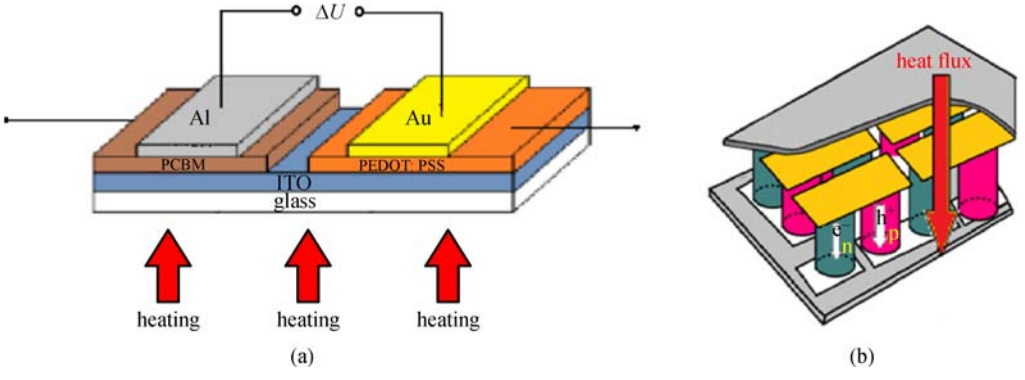

Fig. 2 (a) Schematic diagram of p- and n-type organic TE devices structure in heating conditions: ITO/PEDOT:PSS/Au + ITO/PCBM/ Al thermocouple device and (b) TE module schematic diagram

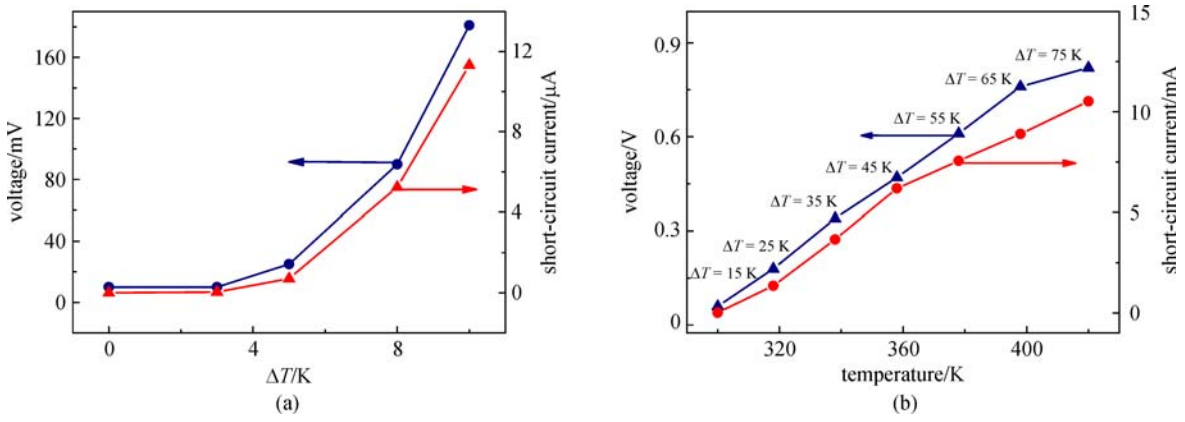

Fig. 3 Output voltage and short-circuit current of (a) single p-and n-type thermocouple devices under various temperatures; (b) thermocouple modules device under various hot-side temperatures

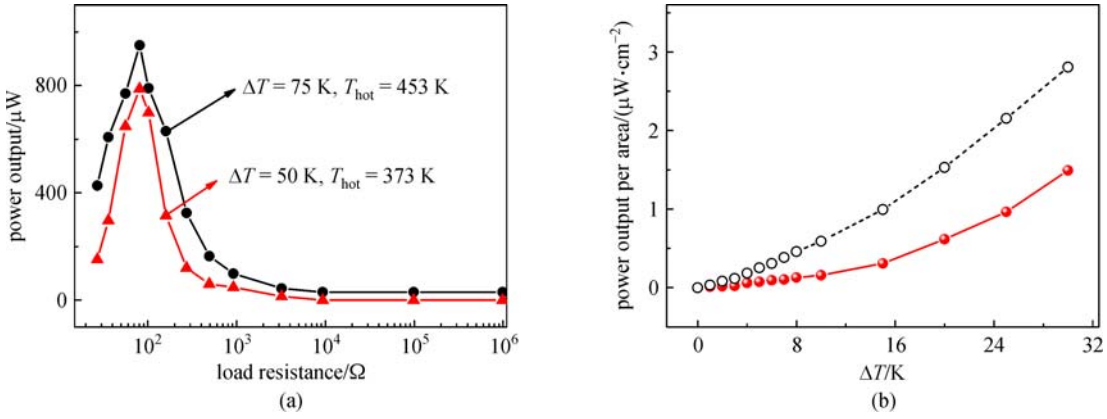

Fig. 4 (a) Useful power output of PEDOT:PSS and PCBM thermocouple devices with various resistance loads were measured at hot-side temperature of 373 and 453 K, respectively. Temperature differences reached 50 and 75 K, respectively. (b) Maximum output power per area of PEDOT:PSS/PCBM TEGs consisting of 48 thermocouples legs. (Matrix packing density defined as the area occupied by legs over total area of TEG of 0.48). Extrapolated limit power output for packing density of 0.94 is plotted with a dashed line

PEDOT:PSS thermocouple model. Assuming optimal packing density of legs (dashed line 1 in Fig. 4), the highest expected electrical power generation from such modules was extrapolated to 2.81 μW/cm^2 at Δt = 30 K.

TE module showed good stability. We tested stability of power with increasing time and observed that under ambient atmosphere, it did not degrade after 2800 min at high temperature of 373 K, as shown in Fig. 5. Deduced half-lifetime is longer than 50 h.

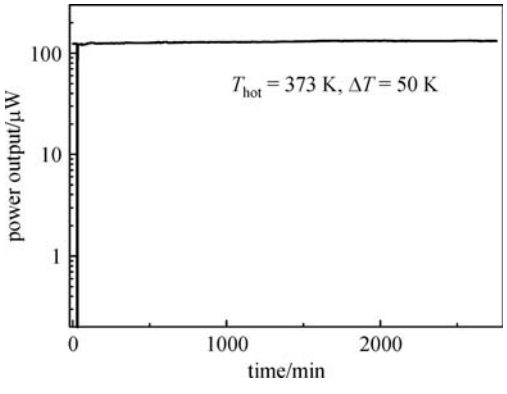

Fig. 5 Output power stability of TE device with hot-side temperature of 373 K and temperature difference of 50 K

4 Conclusions

PCBM were doped with AOB or N-DMBI as n-type legs in TE module. In codoped samples, synergistic effects of AOB and N-DMBI can simultaneously increase electrical conductivity and Seebeck coefficient compared with single-doped and undoped PCBM samples. Electrical conductivity reached 2 S/cm, and obtained Seebeck coefficients were as large as −500 μV/K when dopant molar ratio was 0.11. These characteristics remained almost constant when samples were placed in air

environment for 2 days. Based on these p-type (PEDOT: PSS) and n-type (PCBM) TE materials, a TE module consisting of 48 thermocouple legs were fabricated. Upon application of a 75 K temperature gradient, maximum TE voltage measured 0.82 V at hot-side temperature of 453 K. Although efficiency of organic TE devices is still much lower than state-of-the-art inorganic TE devices, it can be further increased by device optimization. Organic TE devices also feature many advantages, including facile synthesis, being light-weight, low-cost, and non-toxicity. These results can promote organic TE materials and devices and their development and application in green energy field.

Acknowledgements We acknowledge the financial support provided by the National Young Natural Science Foundation of China (Grant No. 61306067) and the Fundamental Research Funds for the Central Universities in Huazhong University of Science and Technology (Nos. 2014NY009 and 2016YXMS033).

References

1. Venkatasubramanian R, Siivola E, Colpitts T, O'Quinn B. Thin-film thermoelectric devices with high room-temperature figures of merit. Nature, 2001, 413(6856): 597–602
2. Zhao D, Tan G. A review of thermoelectric cooling: materials, modeling and applications. Applied Thermal Engineering, 2014, 66 (1-2): 15–24
3. Zhao L D, Tan G J, Hao S Q, He J Q, Pei Y, Chi H, Wang H, Gong S, Xu H, Dravid V P, Uher C, Snyder G J, Wolverton C, Kanatzidis M G. Ultrahigh power factor and thermoelectric performance in hole doped single-crystal SnSe. Science, 2016, 351(6269): 141–144
4. Yan L, Shao M, Wang H, Dudis D, Urbas A, Hu B. High Seebeck effects from hybrid metal/polymer/metal thin-film devices. Advanced Materials, 2011, 23(35): 4120–4124
5. Taggart D K, Yang Y, Kung S C, McIntire T M, Penner R M. Enhanced thermoelectric metrics in ultra-long electrodeposited PEDOT nanowires. Nano Letters, 2011, 11(1): 125–131
6. Bubnova O, Khan Z U, Malti A, Braun S, Fahlman M, Berggren M, Crispin X. Optimization of the thermoelectric figure of merit in the conducting polymer poly(3,4-ethylenedioxythiophene). Nature Materials, 2011, 10(6): 429–433
7. Zhang Q, Sun Y M, Xu W, Zhu D B. Thermoelectric energy from flexible P3HT films doped with a ferric salt of triflimide anions. Energy & Environmental Science, 2012, 5(11): 9639–9644
8. Ma H K, Lin C P, Wu H P, Peng C H, Hsu C C. Waste heat recovery using a thermoelectric power generation system in a biomass gasifier. Applied Thermal Engineering, 2015, 88: 274–279
9. Bubnova O, Crispin X. Towards polymer-based organic thermoelectric generators. Energy & Environmental Science, 2012, 5(11): 9345–9362
10. Bubnova O, Berggren M, Crispin X. Tuning the thermoelectric properties of conducting polymers in an electrochemical transistor. Journal of the American Chemical Society, 2012, 134(40): 16456–16459
11. Poehler T O, Katz H E. Prospects for polymer-based thermoelectrics: state of the art and theoretical analysis. Energy & Environmental Science, 2012, 5(8): 8110–8115
12. Jiao F, Di C A, Sun Y, Sheng P, Xu W, Zhu D B. Inkjet-printed flexible organic thin-film thermoelectric devices based on p- and n-type poly(metal 1,1,2,2-ethenetetrathiolate)s/polymer composites through ball-milling. Philosophical Transactions of the Royal Society A, 2014, 372(2013): 20130008
13. Yu C, Murali A, Choi K, Ryu Y. Air-stable fabric thermoelectric modules made of N- and P-type carbon Nanotubes. Energy & Environmental Science, 2012, 5(11): 9481–9486
14. Shen S, Henry A, Tong J, Zheng R, Chen G. Polyethylene nanofibres with very high thermal conductivities. Nature Nanotechnology, 2010, 5(4): 251–255
15. Rojo M M, Martín J, Grauby S, Borca-Tasciuc T, Dilhaire S, Martin-Gonzalez M. Correction: Decrease in thermal conductivity in polymeric P3HT nanowires by size-reduction induced by crystal orientation: new approaches towards thermal transport engineering of organic materials. Nanoscale, 2015, 7(9): 4256–4257
16. Hansen D, Bernier G A. Thermal conductivity of polyethylene: the effects of crystal size, density and orientation on the thermal conductivity. Polymer Engineering and Science, 1972, 12(3): 204–208
17. See K C, Feser J P, Chen C E, Majumdar A, Urban J J, Segalman R A. Water-processable polymer-nanocrystal hybrids for thermoelectrics. Nano Letters, 2010, 10(11): 4664–4667
18. Yu C, Choi K, Yin L, Grunlan J C. Light-weight flexible carbon nanotube based organic composites with large thermoelectric power factors. ACS Nano, 2011, 5(10): 7885–7892
19. Bubnova O, Khan Z U, Wang H, Braun S, Evans D R, Fabretto M, Hojati-Talemi P, Dagnelund D, Arlin J B, Geerts Y H, Desbief S, Breiby D W, Andreasen J W, Lazzaroni R, Chen W M, Zozoulenko I, Fahlman M, Murphy P J, Berggren M, Crispin X. Semi-metallic polymers. Nature Materials, 2014, 13(2): 190–194
20. Culebras M, Gómez C M, Cantarero A. Enhanced thermoelectric performance of PEDOT with different counter-ions optimized by chemical reduction. Journal of Materials Chemistry A, Materials for Energy and Sustainability, 2014, 2(26): 10109–10115
21. Lee G W, Park M, Kim J, Lee J I, Yoon H G. Enhanced thermal conductivity of polymer composites filled with hybrid filler. Composites Part A, Applied Science and Manufacturing, 2006, 37 (5): 727–734
22. Stankovich S, Dikin D A, Dommett G H B, Kohlhaas K M, Zimney E J, Stach E A, Piner R D, Nguyen S T, Ruoff R S. Graphene-based composite materials. Nature, 2006, 442(7100): 282–286
23. Kilbride B E, Coleman J N, Fraysse J, Fournet P, Cadek M, Drury A, Hutzler S, Roth S, Blau W J. Experimental observation of scaling laws for alternating current and direct current conductivity in polymer-carbon nanotube composite thin films. Journal of Applied Physics, 2002, 92(7): 4024–4030
24. Cho C, Stevens B, Hsu J H, Bureau R, Hagen D A, Regev O, Yu C, Grunlan J C. Completely organic multilayer thin film with thermoelectric power factor rivaling inorganic tellurides. Advanced Materials, 2015, 27(19): 2996–3001
25. Wei Q, Mukaida M, Kirihara K, Naitoh Y, Ishida T. Recent progress on PEDOT-based thermoelectric materials. Materials (Basel), 2015,

8(2): 732–750
26. Bae E J, Kang Y H, Jang K S, Cho S Y. Enhancement of thermoelectric properties of PEDOT: PSS and tellurium-PEDOT: PSS hybrid composites by simple chemical treatment. Scientific Reports, 2016, 6(1): 18805–18815
27. Schlitz R A, Brunetti F G, Glaudell A M, Miller P L, Brady M A, Takacs C J, Hawker C J, Chabinyc M L. Solubility-limited extrinsic n-type doping of a high electron mobility polymer for thermoelectric applications. Advanced Materials, 2014, 26(18): 2825–2830
28. Russ B, Robb M J, Brunetti F G, Miller P L, Perry E E, Patel S N, Ho V, Chang W B, Urban J J, Chabinyc M L, Hawker C J, Segalman R A. Power factor enhancement in solution-processed organic n-type thermoelectrics through molecular design. Advanced Materials, 2014, 26(21): 3473–3477
29. Dang M T, Hirsch L, Wantz G. P3HT:PCBM, best seller in polymer photovoltaic research. Advanced Materials, 2011, 23(31): 3597–3602
30. Chen D, Nakahara A, Wei D, Nordlund D, Russell T P. P3HT/PCBM bulk heterojunction organic photovoltaics: correlating efficiency and morphology. Nano Letters, 2011, 11(2): 561–567
31. Seo J, Park S, Chan Kim Y, Jeon N J, Noh J H, Yoon S C, Seok S I. Benefits of very thin PCBM and LiF layers for solution-processed p–i–n perovskite solar cells. Energy & Environmental Science, 2014, 7(8): 2642–2646
32. Ye L, Zhang S Q, Qian D P, Wang Q, Hou J H. Application of bis-PCBM in polymer solar cells with improved voltage. Journal of Physics Chemistry C, 2013, 117: 25360–25366
33. Ye L, Fan B H, Zhang S Q, Li S S , Yang B, Qin Y P, Hao Z, Hou J H. Perovskite-polymer hybrid solar cells with near-infrared external quantum efficiency over 40%. Science China Materials, 2015, 58: 953–960
34. Menke T, Ray D, Meiss J, Leo K, Riede M. In-situ conductivity and Seebeck measurements of highly efficient n-dopants in fullerene C_{60}. Applied Physics Letters, 2012, 100(9): 093304
35. Schafferhans J, Baumann A, Wagenpfahl A, Deibel C, Dyakonov V. Oxygen doping of P3HT: PCBM blends: influence on trap states, charge carrier mobility and solar cell performance. Organic Electronics, 2010, 11(10): 1693–1700
36. Lee H W, Yoon Y, Park S, Oh J H, Hong S, Liyanage L S, Wang H, Morishita S, Patil N, Park Y J, Park J J, Spakowitz A, Galli G, Gygi F, Wong P H, Tok J B, Kim J M, Bao Z. Selective dispersion of high purity semiconducting single-walled carbon nanotubes with regioregular poly(3-alkylthiophene)s. Nature Communications, 2011, 2: 541
37. Gomulya W, Costanzo G D, de Carvalho E J F, Bisri S Z, Derenskyi V, Fritsch M, Fröhlich N, Allard S, Gordiichuk P, Herrmann A, Marrink S J, dos Santos M C, Scherf U, Loi M A. Semiconducting single-walled carbon nanotubes on demand by polymer wrapping. Advanced Materials, 2013, 25(21): 2948–2956
38. Menke T, Wei P, Ray D, Kleemann H, Naab B D, Bao Z, Leo K, Riede M. A comparison of two air-stable molecular n-dopants for C_{60}. Organic Electronics, 2012, 13(12): 3319–3325
39. Li F, Pfeiffer M, Werner A, Harada K, Leo K, Hayashi N, Seki K, Liu X, Dang X D. Acridine orange base as a dopant for n doping of C_{60} thin films. Journal of Applied Physics, 2006, 100(2): 023716
40. Allard S, Forster M, Souharce B, Thiem H, Scherf U. Organic semiconductors for solution-processable field-effect transistors (OFETs). Angewandte Chemie, 2008, 47(22): 4070–4098
41. Di C A, Zhang F, Zhu D. Multi-functional integration of organic field-effect transistors (OFETs): advances and perspectives. Advanced Materials, 2013, 25(3): 313–330
42. Rovira C. Bis(ethylenethio)tetrathiafulvalene (BET-TTF) and related dissymmetrical electron donors: from the molecule to functional molecular materials and devices (OFETs). Chemical Reviews, 2004, 104(11): 5289–5318

Feng Gao graduated with a B.S. degree in optical information science and technology at Shanxi University in 2014. He is a master's degree student in optical engineering at Huazhong University Science and Technology (2014 to 2017). Currently, his research focuses on organic thermoelectric materials and devices.

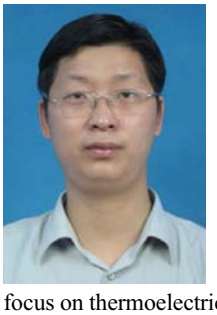

Ling Xu received his M.S. and Ph.D. degrees from Huazhong University Science and Technology in 2007 and 2010, respectively. He became a full associate professor in Wuhan National Laboratory of Optoelectronics at Huazhong University Science and Technology in 2015. He is a lifelong member of Society of Photo-Optical Instrumentation Engineers. His interests mainly focus on thermoelectric materials and devices and energy conversion and application fields.